# *Non-aqueous electrolytes for isotachophoresis of weak bases and its application to the comprehensive preconcentration of the 20 proteinogenic amino acids in column-coupling ITP/CE–MS*

**Pablo A. Kler & Carolin Huhn**

**Analytical and Bioanalytical Chemistry**

ISSN 1618-2642
Volume 406
Number 28

Anal Bioanal Chem (2014)
406:7163-7174
DOI 10.1007/s00216-014-8152-6

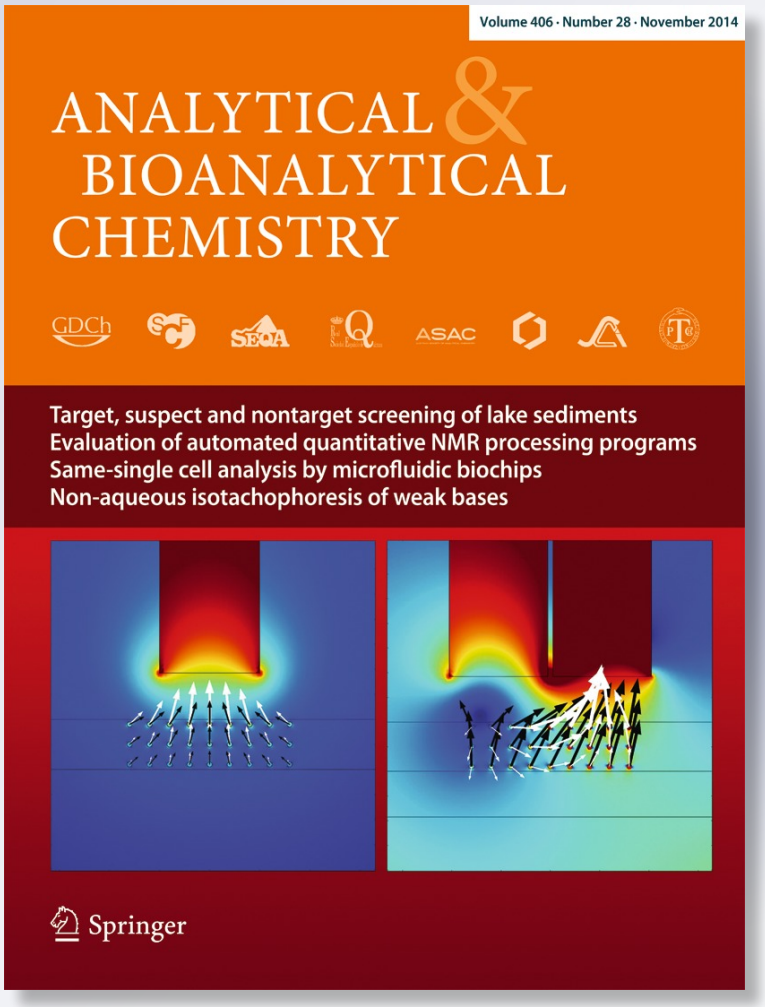


Springer

Anal Bioanal Chem (2014) 406:7163–7174
DOI 10.1007/s00216-014-8152-6

RESEARCH PAPER

# Non-aqueous electrolytes for isotachophoresis of weak bases and its application to the comprehensive preconcentration of the 20 proteinogenic amino acids in column-coupling ITP/CE–MS

**Pablo A. Kler · Carolin Huhn**

Received: 5 June 2014 / Revised: 26 August 2014 / Accepted: 1 September 2014 / Published online: 27 September 2014


**Abstract** Isotachophoresis (ITP) has long been used alone but also as a preconcentration technique for capillary electrophoresis (CE). Unfortunately, up to now, its application is restricted to relatively strong acids and bases as either the degree of (de)protonation is too low or the water dissociation is too high, evoking zone electrophoresis. With the comprehensive ITP analysis of all 20 proteinogenic amino acids as model analytes, we, here, show that non–aqueous ITP using dimethylsulfoxide as a solvent solves this ITP shortcoming. Dimethylsulfoxide changes the pH regime of analytes and electrolytes but, more importantly, strongly reduces the proton mobility by prohibiting hydrogen bonds and thus, the so-called Zundel–Eigen–Zundel electrical conduction mechanism of flipping hydrogen bonds. The effects are demonstrated in an electrolyte system with taurine or $H^+$ as terminator, and imidazole as leader together with strong acids such as oxalic and even trifluoroacetic acid as counterions, both impossible to use in aqueous solution. Mass spectrometric as well as capacitively coupled contactless conductivity detection ($C^4D$) are used to follow the ITP processes. To demonstrate the preconcentration capabilities of ITP in a two-dimensional set-up, we, here, also demonstrate that our non-aqueous ITP method can be combined with capillary electrophoresis–mass spectrometry in a column-coupling system using a hybrid approach of capillaries coupled to a microfluidic interface. For this, $C^4D$ was optimized for on-chip detection with the electrodes aligned on top of a thin glass lid of the microfluidic chip.

**Keywords** Non-aqueous isotachophoresis · Capacitively coupled contactless conductivity detection · ITP/CE-MS · Weak bases · Amino acids

ABC Highlights: authored by *Rising Stars and Top Experts*

**Electronic supplementary material** The online version of this article (doi:10.1007/s00216-014-8152-6) contains supplementary material, which is available to authorized users.

P. A. Kler (✉) · C. Huhn (✉)
Institute of Physical and Theoretical Chemistry,
Faculty of Science, Eberhard Karls Universität Tübingen,
Auf der Morgenstelle 18, 72076, Tübingen, Germany
e-mail: pablo-alejandro.kler@uni-tuebingen.de
e-mail: carolin.huhn@uni-tuebingen.de

## Introduction

Isotachophoresis (ITP) is an electromigrative separation and preconcentration technique that has been extensively used for the analysis of different biomolecules [1]. ITP offers ideal bioanalytical features in terms of its high sample loadability and its strong preconcentration effect, thus giving rise to impressive limits of detection with excellent quantification possibilities via capacitively coupled contactless conductivity detection ($C^4D$), and full compatibility with electrospray ionization–mass spectrometry (ESI-MS) for analyte identification [2]. Additionally, ITP enables efficient matrix removal particularly for compounds with high effective electrophoretic mobilities usually present in biological samples such as sodium and chloride [3].

The analysis of amino acids using ITP has been implemented using both transient ITP (tITP) for on-line preconcentration, and column ITP (cITP) using ad hoc ITP devices or standard capillary electrophoresis (CE) equipment [4, 5]. tITP-CE analysis of amino acids has been implemented for

on-line preconcentration in several studies involving sets of up to 11 different amino acids [6, 7]. In the case of cITP, different studies for the analysis of amino acids have been published for selected amino acids or for small subsets such as the three basic ones (arginine, lysine and histidine), or the two acidic ones (aspartic acid and glutamic acid) [8]. At present, the inclusion of 20 proteinogenic amino acids in a single ITP method was not achieved mainly due to the difficulties in satisfying ITP conditions for this heterogeneous group of molecules.

In order to have all the amino acids ionized (all of them as cations or all as anions), it is mandatory to work at extreme pH values where ITP conditions cannot be reached using aqueous solutions. At low pH (e.g. pH = 2–3), amino acids will migrate as cations; however, especially glutamate and aspartate have a too low effective electrophoretic mobility to be stacked. This is due to the high effective electrophoretic mobility of $H^+$ in electrolyte systems of low pH, thus it is faster than the low-mobility analytes excluding them from the ITP stack and leaving them moving electrophoretically in the terminator. The same holds true at high pH with $OH^-$ ions for lysine and arginine [9].

In this study, we will show that non-aqueous (NA) or aqueous-organic electrolytes using the dipolar aprotic solvent dimethylsulfoxide (DMSO) can be employed to allow also weak bases and ampholytes of low pI to be incorporated in the ITP mobility window spanned by leading and terminating electrolyte in isotachophoresis. As model analytes, we chose the 20 proteinogenic amino acids due to their broad pI and mobility range as well as the large number of published reference methods [10].

We present the development of an NAITP-$C^4$D-MS method based on DMSO solutions as a main solvent using $C^4$D detection for sensing the conductivities of NAITP steps and MS for the unambiguous identification of the different analytes. These measurements also enabled us to understand the underlying physicochemical phenomena involved in the NAITP shown in this study. As an application example, the developed NAITP method was included in a comprehensive NAITP-on-chip-$C^4$D/CE-MS method using a previously presented hybrid capillary-microchip two-dimensional system [11].

## Materials and methods

### Chemicals, reagents and solvents

Taurine, 2-propanol, methanol, trifluoroacetic acid (TFA) and the 20 L-amino acids were bought from Fluka (Steinheim, Germany), and DMSO (EMPLURA® > 99 %), glacial acetic acid, hydrochloric acid, sodium hydroxide, imidazole and oxalic acid from Merck (Darmstadt, Germany). All aqueous solutions were prepared with water from a Millipore Milli-Q purification system (Bedford, MA, USA). Following the information in the data sheets provided by the supplier, amino acid 200 mM stock solutions were prepared using 1 M purely aqueous HCl solution for methionine, asparagine, glutamine, valine, tyrosine, aspartic acid and glutamic acid; 1 M purely aqueous NaOH solution for lysine, leucine, and tryptophan and the rest were prepared using DI water as solvent. In the case of phenylalanine, the water-based solution was heated to 80 °C for 5 min to achieve complete dissolution.

For all the experiments, sheath liquid was water/2-propanol solution (50:50) with 1 % glacial acetic acid and 0.1 % imidazole oxalate 10 mM. Sheath liquid was used after 10 min of ultrasonication. The addition of LE and CI to the sheath liquid provides a higher homogeneity in the electric conductivity profile of the whole electric circuit, providing conditions for ITP until the end of the column, supplying counterions, and enabling us to perform direct ESI-MS detection of cationic ITP avoiding the use of external hydrodynamic pressure for step mobilization or using the suction effect induced by the nebulizer of the ESI [12].

### NAITP-$C^4$D-MS

NAITP-$C^4$D-MS separations were performed using an Agilent 7100 CE system (Agilent Technologies, Waldbronn, Germany) providing pressure and voltage regimes, injection control and vial handling. MS detection was achieved using an Agilent 6340 Ion Trap (Agilent Technologies, Santa Clara, CA, USA). The CE was coupled to the MS via a coaxial sheath liquid interface CE-MS adapter-kit (Agilent Technologies, Santa Clara, CA, USA) using an Agilent isocratic pump 1260 (Agilent Technologies, Waldbronn, Germany) for delivering sheath liquid at a constant volume rate of 4 µL/min. Ion trap settings were: 5 L/min drying gas were supplied at 300 °C, nebulizer gas flow at a rate of 6 L/min, and *smart parameter settings* were optimized for a mean m/z value of 180. Maximum accumulation time was 200 ms and the *ion charge control* was set to 500,000. Fused silica capillaries of 100-µm inner diameter and 60-cm length, purchased from Polymicro Technologies (Phoenix, AZ, USA), were used for this application.

Experimental conditions for NAITP-$C^4$D-MS were: preconditioning with 5-min flushing with 50:50 water/methanol solution at 3 bar, and 5-min flushing with LE solution at 3 bar; injection at 50 mbar for 5 s; separation at 30 kV. Due to the fact that our work did not focus on the quantification properties of ITP, we worked at constant voltage instead of the recommended constant current [8], obtaining, in this way, shorter analysis times. For these series of measurements, sample concentration was 10 µm for each amino acid, dissolved in a water–DMSO solution,

with the same content of DMSO as the LE and TE buffers. High pressure values for flushing (3 bar) were employed due to the high viscosity of the aqueous–DMSO solutions (see Table 1 in the Supplementary Material).

### $C^4D$ detection

$C^4D$ detection was performed using a CSense One detection system (CalvaSens GmbH, Aalen, Germany) using two different detector heads: one for capillaries and one for microfluidic chips. For the NAITP-$C^4D$-MS experiments, the $C^4D$ detector capillary head was placed right at the fixation nut of the ESI sprayer, resulting in an effective detection length of 49 cm. The $C^4D$ detector head for microfluidic chips consisted of a normal electronic printed circuit board with the detection and shielding electrodes imprinted on its surface. These electrodes were aligned to the common channel of the glass microfluidic chip using an Olympus IX-81 inverted optical microscope (Olympus Corporation, Tokyo, Japan), then the board and the chip were fixated using hot melt adhesive to keep them aligned.

### Software

The CE unit was controlled by ChemStation® B.04.02 (Agilent Technologies, Santa Clara, CA, USA). The ion trap was operated with the 6300 Series TrapControl Version 6.2 (Agilent Technologies, Santa Clara, CA, USA). Data evaluation was performed with Agilent Data Analysis 6.2 (Bruker Daltonik GmbH, Bremen, Germany). Ion electropherograms were extracted with ±30 ppm accuracy. Numerical simulations were performed using a previously developed finite element method using the program PETSc-FEM as platform [13, 14]. The simulations were performed on a desktop computer provided with a quad-core Intel i7 3770 3.4 GHz processor, QuickPath interconnect, 16 GB DDR3-1066 memory.

### NAITP-$C^4D$/CE-MS

For the NAITP-on-chip-$C^4D$/CE-MS we used a hybrid capillary-microchip system [11]. The interface between fused sillica capillaries was an in-house designed and customized manufactured glass microfluidic chip (iX-factory GmbH, Dortmund, Germany), similar to the one shown in Fig. 1a. The microfluidic network was made in Borofloat glass, the channels had a width of 60 µm and a depth of 25 µm, and were configured as a double-T with a common channel of 5-mm length (see Fig. 1b). The thickness of the top glass wafer was only 200 µm enabling on-chip $C^4D$ detection using external electrodes mounted in the detector head as shown in Fig. 1b. The fabrication protocol of these glass chips and the capillary to chip coupling were similar to the procedure described in [15]. The capillaries were of 100-µm inner diameter for the NAITP separation and 50-µm diameter for the second dimension (CE separation). Capillary length was 35 cm for all four segments.

NAITP-on-chip-$C^4D$/CE-MS separations were performed using a home-made multivial holder. This holder enabled the simultaneous and independent control of pressure and high voltage regimes for four vials, plus a chip holder that enabled the on-chip $C^4D$ detection. We employed the Agilent CE 7100 system for controlling and supplying pressure, both for injection and flushing, via by-passing the pneumatic connection of the inlet port. Pneumatic valves Festo MFH-3-M5 (FESTO AG, Neuss, Germany) were controlled manually with an ad hoc switch module. For the high voltage regime, we used a custom-made multiport HV source (CalvaSens GmbH, Aalen, Germany) that enabled the independent operation of 12 high voltage channels, 6 positive channels (from 0 to 15 kV) and six negative (from −15 to 0 kV).

Experimental conditions included four preconditioning steps: (i) flushing the whole circuit (capillaries plus chip) with 50:50 water/methanol solution at 3 bar for 5 min from Port 2, (ii) flushing with LE at 3 bar for 2 min from Port 2, (iii) blocking the capillary ends at Ports 2 and 3 using silicone blockers integrated into the CE vials and (iv) low pressure injection (100 mbar) of CE buffer from Port 1 until the signal of imidazole in the MS significantly decreases (usually 4.5 min) indicating the complete filling of the CE-MS channel with background electrolyte (BGE).

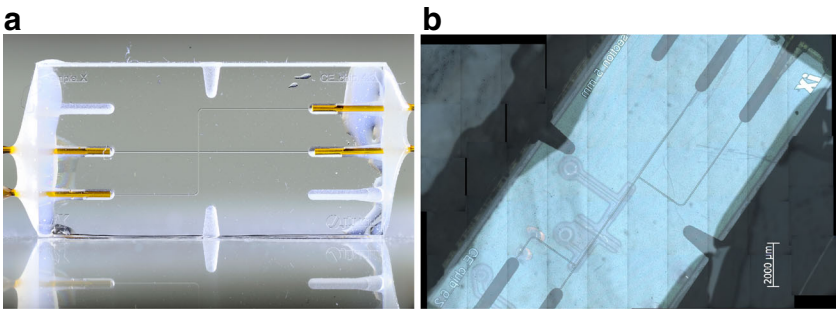


**Fig. 1** Customized setup for performing NAITP/on-chip-$C^4D$-CE/MS. (**a**) Example of the capillary to chip coupling using a cross configuration. (**b**) On-chip $C^4D$ detection head–glass chip assembly on a chip with double-T configuration

In this case, CE buffer was 20 mM oxalic acid in a solution of 80:20 water/2-propanol. The aim of the addition of 2-propanol to the CE-BGE was to approximate its viscosity to the NAITP electrolytes that contained 80 % of DMSO [16]. Injection parameters were 100 mbar for 7 s. Sample concentration was also 10 µm for each amino acid, dissolved in a water–DMSO solution, with 80 % DMSO.

After preconditioning and sample injection using Port 2, the two-dimensional separation was carried out involving three different steps as shown in Fig. 2: (i) the first preconcentration step (NAITP) was performed by applying +15 kV at Port 2 and −15 kV at Port 3 (Fig. 2a). (ii) When the on-chip $C^4D$ signal indicated that the sample stack from the intersection reached the microfluidic chip (i.e. a drop in the electric conductivity equal to 50 % of the electric conductivity gap between LE and TE), the potential in Port 3 was switched to float and the second step (transfer) was carried out. In the transfer step, +15 kV were applied only at Port 2 for 2 min in order to ensure the proper transfer of the sample stack from the ITP channel to the CE channel (Fig. 2b). (iii) Once the sample stack was transferred, we started the third step (CE) by applying +15 kV to Port 1 until all the sample components were detected by the MS (Fig. 2c).

## Results

### NAITP-$C^4D$-MS

The development of a successful NAITP system for the comprehensive analysis of 20 proteinogenic amino acids involved two different stages. The first was devoted to define a pure aqueous buffer system that enables cationic migration of all amino acids by satisfying the ITP Condition (1):

$$|\mu_{LE}| > |\mu_{A_1}| > \ldots > |\mu_{A_n}| > |\mu_{TE}| > 0, \quad (1)$$

where $\mu_{LE}$, $\mu_{TE}$ and $\mu_{A_j}$ represent the effective electrophoretic mobilities of the LE, TE and the different analytes ($A_j$), respectively. Please refer to Tables 1 and 2, and Supplementary Material for further details about the application of this condition and the related theoretical considerations.

The second stage consisted in finding a suitable solvent composition in order to satisfy the ITP Condition (2):

$$\kappa_{LE} > \kappa_{A_1} > \ldots > \kappa_{A_n} > \kappa_{TE} \gg (\kappa_{CI} + \kappa_{H^+}) > 0. \quad (2)$$

where $\kappa$ represents the electrical conductivities of LE ($\kappa_{LE}$), TE ($\kappa_{TE}$), CI ($\kappa_{CI}$), $H^+$ ($\kappa_{H^+}$) and analytes ($\kappa_{A_j}$),

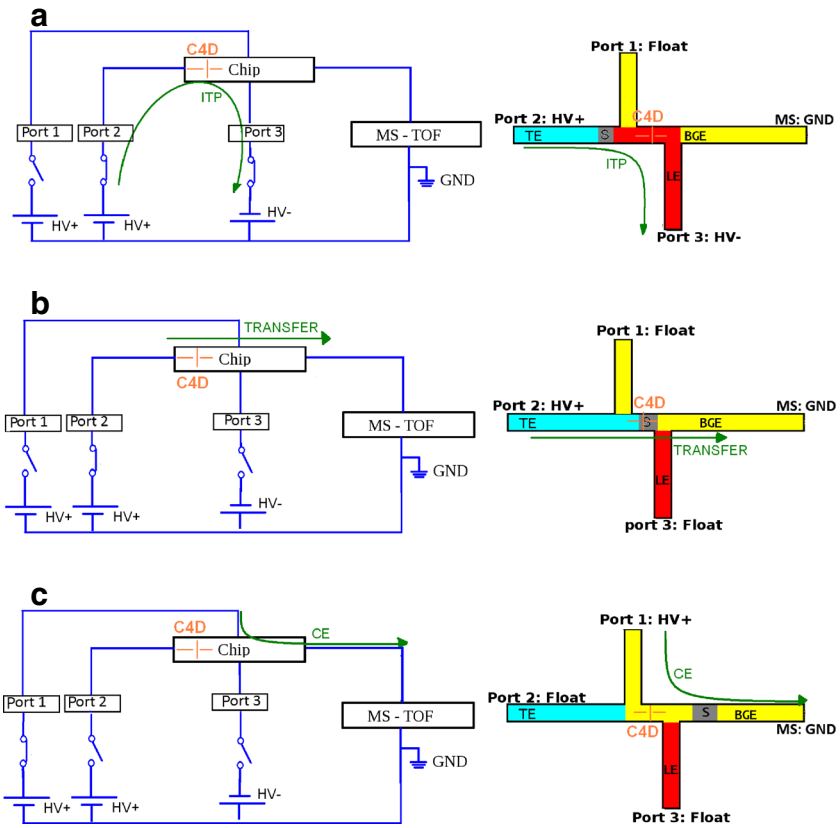


**Fig. 2** Electrical circuit and operational scheme for the three different steps involved in the two-dimensional electrophoretic separation. (**a**) NAITP; (**b**) transfer; (**c**) CE

**Table 1** Composition of the two numerically designed electrolyte systems and predicted aqueous pH and zone conductivities

| | Electrolyte system A | | | | | Electrolyte system B | | | | |
|---|---|---|---|---|---|---|---|---|---|---|
| | Compound | Conc. [mM] | $\kappa$ $[S/m]$ | $\kappa_{H^+}$ $[S/m]$ | pH | Compound | Conc. [mM] | $\kappa$ $[S/m]$ | $\kappa_{H^+}$ $[S/m]$ | pH |
| LE | Imidazole | 10 | 0.046 | 0.387 | 1.993 | Imidazole | 10 | 0.045 | 0.751 | 1.711 |
| CI | Oxalic acid | 25 | 0.078 | | | TFA | 35 | 0.116 | | |
| TE | Taurine | 10 | 0.0085 | 0.357 | 2.025 | Taurine | 10 | 0.011 | 0.524 | 1.859 |
| CI | Oxalic acid | 15 | 0.048 | | | TFA | 20 | 0.067 | | |

respectively. For further details about the application of this condition and the related theoretical considerations, please refer to the Supplementary Material.

In order to satisfy Condition (1), we numerically simulated the initial conditions of a pure aqueous ITP system at the defined working pH to determine the conductivities and the effective electrophoretic mobilities of LE, TE and analytes in the aqueous solution. The results of this numerical experiment enabled us to select the suitable counterion taking into account the target working pH of 1.95. Three suitable candidates with good buffering capacity at the working pH were: oxalate, trichloroacetate and trifluoroacetate. Trichloroacetate had to be discarded as it suffers successive decarboxylations to form chloroform in a reaction catalyzed by DMSO [17]. For the other two counterions, we numerically designed two different electrolyte systems using imidazole as LE and taurine as TE. Besides the suitable effective electrophoretic mobilities of these ions, the selection of these electrolytes was also based on the fact that they present an amino acid-like structure providing the method with a high selectivity, based on a narrow mobility window due to expected similar shifts of the $pK_a$ and effective electrophoretic mobilities. This is particularly important for matrix removal due to the fact that fast cations such as sodium or potassium were outside the calculated ITP window. The characteristics of these two electrolyte systems are shown in Table 1. By comparing the different values of $\kappa_{LE}$, $\kappa_{TE}$, $\kappa_{CI}$ and $\kappa_{H^+}$, it is clear that Condition (2) is not fulfilled as expected from being outside the safe pH region.

**Table 2** Calculated effective electrophoretic mobilities of LE, TE and analytes in the LE and TE pure aqueous electrolyte solutions, for the two electrolyte systems used in this work (see Table 1). Note that Condition (1) is satisfied.

| Compound | Electrolyte system A | | Electrolyte system B | |
|---|---|---|---|---|
| | $\mu_{TE}$ | $\mu_{LE}$ | $\mu_{TE}$ | $\mu_{LE}$ |
| Imidazole (LE) | 48.53 | 47.45 | 48.00 | 46.89 |
| Lysine | 35.18 | 34.37 | 36.66 | 36.86 |
| Histidine | 33.02 | 31.95 | 33.75 | 33.13 |
| Arginine | 32.50 | 32.04 | 34.80 | 36.14 |
| Glycine | 24.90 | 24.97 | 27.35 | 28.64 |
| Alanine | 21.29 | 21.38 | 23.66 | 24.96 |
| Serine | 17.71 | 17.87 | 20.15 | 21.63 |
| Isoleucine | 17.62 | 17.57 | 19.32 | 20.10 |
| Valine | 17.47 | 17.52 | 19.51 | 20.62 |
| Leucine | 17.09 | 17.07 | 18.88 | 19.76 |
| Asparagine | 16.42 | 16.57 | 18.77 | 20.23 |
| Threonine | 16.12 | 16.22 | 18.26 | 19.51 |
| Methionine | 15.33 | 15.41 | 17.39 | 18.58 |
| Tryptophan | 15.31 | 15.19 | 16.71 | 17.26 |
| Glutamine | 15.06 | 15.17 | 17.19 | 18.48 |
| Glutamic acid | 15.03 | 15.11 | 17.06 | 18.21 |
| Phenylalanine | 14.22 | 14.27 | 16.11 | 17.16 |
| Tyrosine | 14.22 | 14.21 | 15.92 | 16.79 |
| Proline | 13.91 | 14.28 | 16.87 | 19.16 |
| Cysteine | 13.41 | 13.73 | 16.17 | 18.25 |
| Aspartic acid | 12.17 | 12.45 | 14.74 | 16.58 |
| Taurine (TE) | 8.66 | 9.06 | 11.33 | 13.86 |

Taking into account the numerically calculated aqueous working pH for the two electrolyte systems chosen, we also determined the effective electrophoretic mobilities for LE, TE and the analytes, verifying that Condition (1) is satisfied. This can be corroborated with the information provided by Table 2: clearly, LE shows the highest effective electrophoretic mobility, TE the smallest and all sample components are in the intermediate range. Due to the differences in pH for LE and TE in both electrolyte systems, Table 2 provides a range of effective electrophoretic mobilities instead of a unique value, nevertheless this variation is small and does not affect the order of the analytes in the mobility window nor the validity of Condition (1).

Once we have verified that the proposed electrolyte systems meet the mobility requirements for ITP Condition (1), we started empirical determination of the solvent composition in order to achieve ITP conditions by satisfying simultaneously Condition (2). This was achieved by reducing the water content of the electrolyte upon addition of

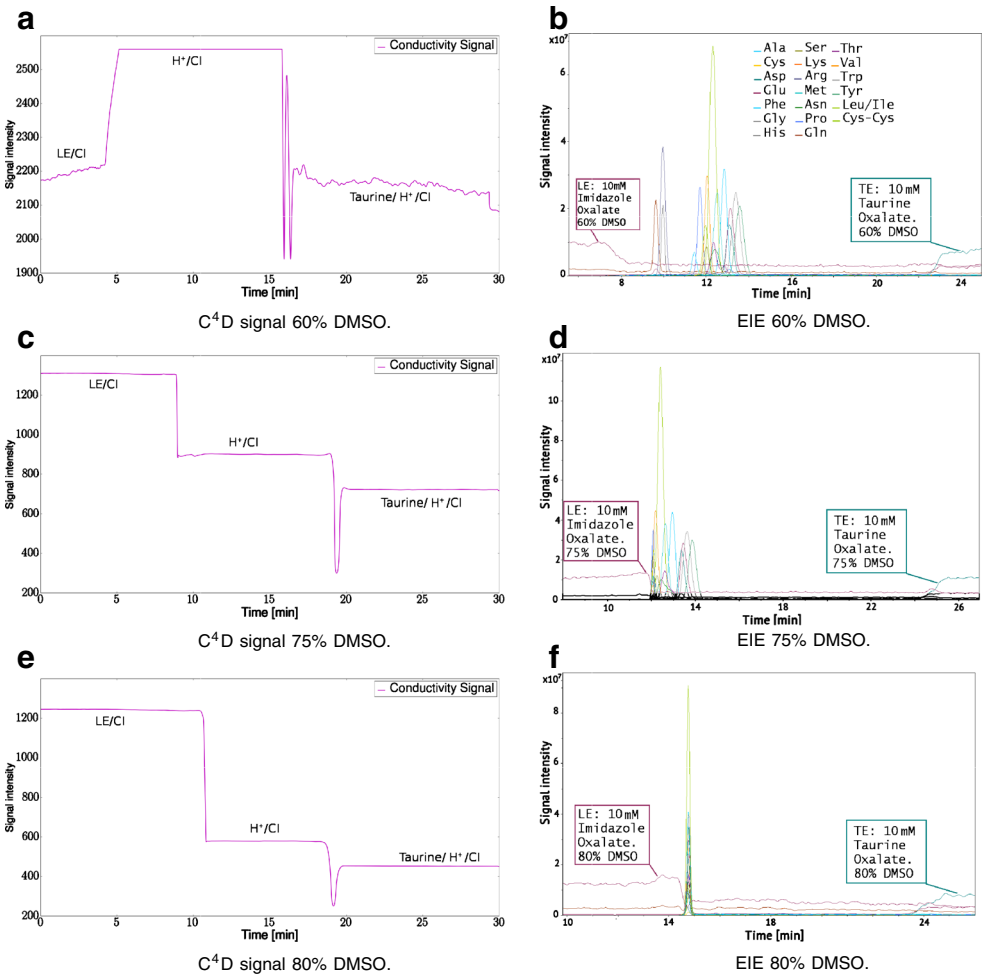


**Fig. 3** NAITP-$C^4D$-MS results, by means of $C^4D$ signal trace and EIE for the LE, TE, the 20 amino acids present in the sample plus cystine, for different contents of DMSO, using electrolyte System A (see Table 1). Hydrodynamic and electrical parameters were: 5 s at 50 mbar for injection, and +30 kV for separation. (**a**) $C^4D$ signal 60 % DMSO. (**b**) EIE 60 % DMSO. (**c**) $C^4D$ signal 75 % DMSO. (**d**) EIE 75 % DMSO. (**e**) $C^4D$ signal 80 % DMSO. (**f**) EIE 80 % DMSO

DMSO. Figure 3 presents the most important results of the first series of experiments in which the percentage of DMSO in the solvent was increased stepwise in the electrolyte System A (oxalic acid as CI) from 50 to 90 %. Panels a, c and e of Fig. 3 show the electric conductivity trace for intermediate contents of DMSO (60, 75 and 80 %). Panels b, d, and f of Fig. 3 show the corresponding mass traces with extracted ion electropherograms (EIE) for LE, TE, the 20 amino acids included in the sample and cystine. Cystine appears as the product of a cysteine dimerization reaction catalyzed due to the presence of DMSO as oxidant under acidic conditions [18, 19]. It is worth mentioning that this reaction is relatively slow, so when samples are prepared immediately prior to the measurement, the cysteine can be analyzed without problems. In our case, samples were prepared once a day and cysteine could be detected up to 30–60 min after the dilution with DMSO.

The combined use of $C^4D$ with MS enabled us to clearly identify the composition of the different detected electric conductivity zones: in Fig. 3a, the electric conductivity of the $H^+$ zone is extremely high, causing the detector signal to overflow. The transitions between high electric conductivity zones to low ones (e.g. transition from $H^+$ to taurine at 16 min in Fig. 3a) generated undershoots and overshoots in the detection system already described in the literature [20]. Increasing the DMSO content to 75 %, it can be seen in Fig. 3c that ITP conditions were reached but having the $H^+$ cation as TE (as read from the MS trace without taurine), and the analytes outside the ITP window. In this case, the analytes were separated by CE in the $H^+$/CI electrolyte system. Finally, Fig. 3f shows that using a solvent with a DMSO content of 80 %, ITP conditions were reached for all analytes, having $H^+$ as TE. Clearly, Condition (2) is now fulfilled.

The second series of experiments was conducted in a similar way as the first one, but using the electrolyte System B (TFA as CI). Figure 4 shows representative isotachopherograms of the second series of experiments in which the percentage of DMSO in the solvent was also stepwise increased but from 50 to 100 %, with panels a, c and e of

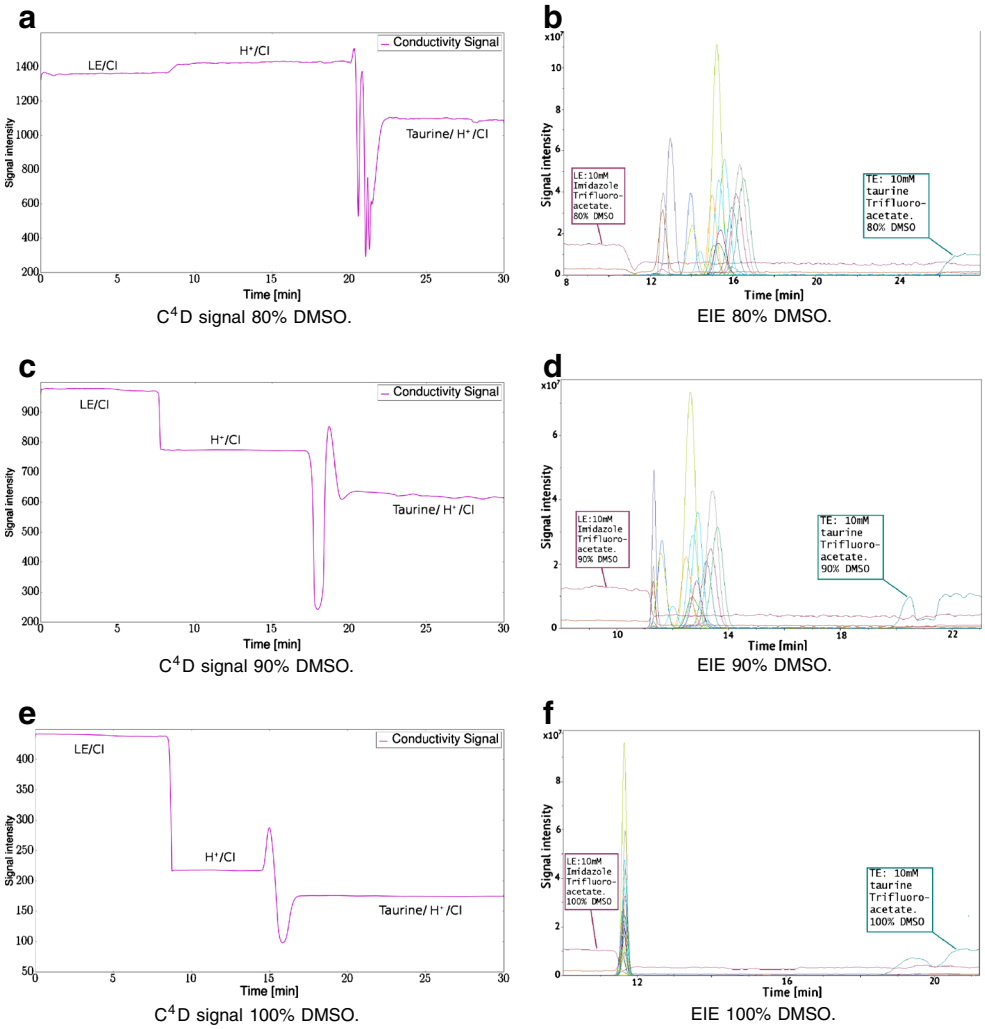


**Fig. 4** NAITP-$C^4D$-MS results, by means of $C^4D$ signal trace and EIE for the LE, TE, the 20 aminoacids present in the sample plus cystine, for different contents of DMSO, using electrolyte System B (see Table 1). Other experimental conditions are similar to the ones presented in Fig. 3. (**a**) $C^4D$ signal 80 % DMSO. (**b**) EIE 80 % DMSO. (**c**) $C^4D$ signal 90 % DMSO. (**d**) EIE 90 % DMSO. (**e**) $C^4D$ signal 100 % DMSO. (**f**) EIE 100 % DMSO

Fig. 4 showing the electric conductivity trace, while panels b, d and e of Fig. 4 show the EIE for LE, TE and the 20 amino acids included in the sample, plus cystine. Experimental conditions and sample concentration for this set of experiments were listed in the previous section and in Table 1.

In Fig. 4a, the electric conductivity of the $H^+$ zone was higher than the LE zone, and no ITP conditions could be observed; instead, the analytes were separated by CE in the $H^+$/CI electrolyte system (taurine signal is negligible in the MS trace). Increasing the DMSO content to 90 %, it can be seen in Fig. 4c that ITP conditions were reached, having the $H^+$ cation as TE, and the fastest analytes (arginine, lysine and histidine) showed a partial stacking process. This means that for these analytes, Condition (2) was satisfied. The other analytes, like in Fig. 4a, were still separated by CE in the $H^+$/CI electrolyte system. Finally, Fig. 4f shows that using pure DMSO as solvent, ITP conditions were reached for all analytes, having $H^+$ as TE.

## Discussion

With the assistance of the numerical simulations, the compositions of the two electrolyte systems were determined in order to satisfy Condition (1) for LE, TE, and the 20 proteinogenic amino acids included in the sample for pure aqueous solutions. These compositions, listed in Table 1, represent a novelty in terms of the use of oxalate and trifluoroacetate as counterions for ITP. In previous works, the most acidic components used as counterions for cationic ITP were caproate or acetate at higher pH values [3, 8], due to the facts that these acids have the buffering point inside the "safe region" (refer to Supplementary Material for a complete description), and thus leading to low values of $\kappa_{CI}$.

Table 1 also shows that for the pure aqueous solution of the calculated electrolyte systems, Condition (2) is absolutely not satisfied due to the fact that $\kappa_{H^+} \gg \kappa_{LE}$ because of the extremely low pH. Also, it is important to note that $\kappa_{CI} > \kappa_{LE}$, due to the fact that we are using strong acids

for the ITP system. It is clear that under these conditions, no ITP would be possible. Using such electrolyte systems in pure aqueous solutions, CE conditions will develop with the $H^+$/CI system as BGE, as was shown in the results of the experiments with low content of DMSO (see Figs. 3a and 4a)

By reducing the water content in the electrolyte system via the addition of DMSO, it is possible to create changes in the $pK_a$ of electrolyte components, and pI of all amino acids in the sample, and, more importantly, decreasing $\mu_{H^+(EZE)}$ due to the replacement of water–water hydrogen bonds and enforcing $H^+$ Stokesian migration, which will be further lowered due to the higher viscosity and the higher autoprotolysis constant of DMSO relative to water. The high electric conductivity of solutions at low pH is not only related to the amount of free $H^+$ ions, but also to the high capability of hydrogen bonds to conduct the electric current. In fact the Stokesian mobility of $H^+$ ions ($\mu_{H^+(Sto)}$) is similar to the mobility of $Li^+$ but the electric conductivity of an aqueous solution of protons is almost ten times higher than the electric conductivity of a solution with the same concentration of $Li^+$ ions [21]. This behavior can be explained taking the proton transfer in water into account: modern models for this transfer state that the stable $[H_3O(3H_2O)]^+$ cation (the Eigen cation) is converted into the transition structure $[H_2O–H–OH_2]^+$ (the Zundel cation) which is finally converted to a new Eigen cation by just flipping hydrogen bonds. This mechanism is known as the Eigen–Zundel–Eigen (EZE) mechanism and results in the propagation of protons along the direction of the electric field with a significantly higher pseudo-mobility ($\mu_{H^+(EZE)} = 306 \times 10^{-9}\ m^2V^{-1}s^{-1}$) than the normal Stokesian migration carried out by solvated protons ($\mu_{H^+(Sto)} = 39 \times 10^{-9}\ m^2V^{-1}s^{-1}$), or any other cation. We can approximate $\kappa_{H^+}$ as follows [22]:

$$\kappa_{H^+} = F\,(\mu_{H^+(Sto)} + \mu_{H^+(EZE)})\,[H^+], \tag{3}$$

were $F$ represents the Faraday constant and $[H^+]$ is the molar concentration of protons in the solution. It is worth mentioning here, that the Stokesian mobility is inversely proportional to the viscosity of the solvent (Walden's rule) and the solvated radius of the proton, whereas the EZE mobility and thus the fast transfer EZE mechanism, is related to the amount of water or other strong protic solvents in the electrolyte in terms of the availability of hydrogen bonds [23].

The addition of DMSO to the buffer for the dilution of water induces physicochemical changes that enable ITP conditions: (a) changes in the electric conductivity profiles of the electrolyte solutions and (b) changes in the effective electrophoretic mobilities of analytes. Although they are closely related, we will discuss them separately. The physicochemical properties of DMSO that enable all these effects are extensively discussed in the Supplementary Material and literature cited there.

*(a) Changes in the electric conductivity profiles* Regarding the selective decrease of electrolyte conductivities, we can state that it is produced due to the interplay of several parameters affecting in different way of each individual $\kappa$:

- $\kappa_{H^+}$: particularly, this electric conductivity is the most affected due to several reasons: (i) with the replacement of the water–water H-bonds, the electric conduction via the EZE mechanism ($\mu_{H^+(EZE)}$) considerably decreases or even approaches zero for contents of solvent higher than 80 %, decreasing the zone electric conductivity by more than 90 % compared to pure aqueous solution [23]; (ii) the Stokesian mobility of $H^+$ ions ($\mu_{H^+(Sto)}$) decreases due to the increase of the viscosity and the decrease of the dielectric constant; (iii) the concentration of $H^+$ ions ($[H^+]$) decreases due to the higher autoprotolysis constant and the shift in the $pK_a$ of the CI acids (to higher values), but also due to the decrease in the solvation capacity of the solvent due to the lower dielectric constant. In this way, all terms in Eq. 3 decrease considerably, consequently decreasing $\kappa_{H^+}$.
- $\kappa_{CI}$: in this case, the zone electric conductivity of CI is also strongly affected due to the shift in $pK_a$. As it is described in the Supplementary Material, in the case of DMSO, this shift is remarkably stronger for acids than for bases. In the same way, $\kappa_{CI}$ decreases due to the low capability of DMSO on solvating anions, but also, due to the increase in the viscosity, and the decrease in the dielectric constant.
- $\kappa_{LE}$: this value is the least affected of the set, due to the low effect of DMSO on shifting $pK_a$ of bases [24] and its good capability for solvating cations (see Supplementary Material). Although, as in the case of the other ions involved, $\kappa_{LE}$ also slightly decreases due to the increase of the viscosity and the decrease of the dielectric constant.
- $\kappa_{TE}$: in this case, due to the amphoteric nature of the TE, the electric conductivity suffers from the aforementioned effects on cations and anions, being different in magnitude: weak for the cationic form and strong for the anionic form. In this case, the strong shift of $pK_{a(-1)}$ compared to the small shift of $pK_{a(+1)}$ causes the decrease of the difference between these two values, increasing the effective charge of the TE.

In Figs. 3a and 4a, the electric conductivity gap between LE and TE was negligible and only CE conditions

developed with $H^+$ as main cation in the BGE: at the beginning and the end of the measurement, electric conductivity signals were similar, due to the prevalence of $\kappa_{CI}$ over $\kappa_{LE}$ and $\kappa_{TE}$. As the DMSO content in the electrolytes increased, the electric conductivity gap was significantly increased, but also, the overall electric conductivity of the different electrolytes decreased in the predicted manner: the change for $\kappa_{LE}$ was relatively small compared to $\kappa_{H^+}$ and $\kappa_{TE}$. In the case of Fig. 3a, we can observe that $H^+$ is acting as BGE in the electrophoretic separation of the amino acids, and in the region between 5 and 15 min, $\kappa_{H^+}$ the electric conductivity signal exceeded the higher detection limit of the $C^4D$.

With the increase in the DMSO content, $\kappa_{H^+}$ and $\kappa_{CI}$ were affected in a way that ITP conditions could develop: In Fig. 3c, we can clearly see the ITP step at 9.5 min showing a clear difference between $\kappa_{LE}$ (first step, electric conductivity level at 1300) and $\kappa_{H^+}$ (second step, electric conductivity level at 900), and $\kappa_{TE}$ (third step, electric conductivity level at 750). In this case, Condition (2) was only fulfilled for LE, but not for analytes, as the proton acted as TE, but due to the high value of $\kappa_{H^+}$, also acted as BGE cation for the zone electrophoretic separation of the amino acids. In the case of panels e and f of Fig. 3, ITP conditions were reached due to the further modification of $\kappa_{LE}$ (electric conductivity level changed from 1300 to 1250), but the more significant modification of $\kappa_{H^+}$ (from 900 to 580) enabling the analytes to enter the ITP mobility window and satisfy Condition (2). Also here, $H^+$ was the TE cation instead of taurine, as far as $\kappa_{TE}$ is also strongly affected as an amphoteric molecule having a lower value than $\kappa_{H^+}$. It is worth mentioning here the importance of the information provided by the MS traces in panels b, d and f of Fig. 3 to understand the behavior of the electrolyte systems, which would not be possible using only the $C^4D$ detection.

In panels a, c and e of Fig. 4, the results were similar, demonstrating our predictions on the effect on the conductivities by the addition of DMSO to the solvent composition. In this case, we have used the electrolyte System B with a stronger acid as CI (TFA). The difference from the results of the experiments with the electrolyte System A, is that the influence of $\kappa_{CI}$ was clearly stronger (compare the different values of $\kappa_{CI}$ in Table 1). In order to satisfy Condition (2) in the presence of a stronger acid, more DMSO was required in order to both lower $\kappa_{H^+}$ and $\kappa_{CI}$ to suitable levels. In this case, the value of $\kappa_{TE}$ was also not high enough in order to have taurine acting as TE, instead $H^+$ ions did, as can directly be inferred from Fig. 4c.

*(b) Changes in the effective electrophoretic mobilities* As a second effect from solvent composition, the changes in the effective electrophoretic mobilities of analytes involves a complex combination of different phenomena that have to be taken into account: (i) due to the combination of the increase of the Stoke's radius or the radius of the solvated molecules (due to the decrease of the dielectric constant of the solvent), and the increase of the viscosity, the absolute mobilities of all analytes decrease; (ii) the effective electrophoretic mobility of analytes is affected due to the selective shift of the $pK_a$ values of the analytes, increasing more strongly the mobilities of the slowest cations with lower $pK_{a(-1)}$ shifting their pI to higher values; and (iii) the decrease of the effective electrophoretic mobilities due to ionic association of fastest cationic analytes and CI anionic molecules.

For the two different electrolyte systems tested, we could corroborate the effect due to the increase in the viscosity, but also the different impact on pI shifting, and ion association phenomena: for the first series of experiments using the electrolyte System A, Fig. 3 clearly shows that the mobility window was narrowed via the relative decrease of the mobilities of the fastest analytes. For example, for imidazole, the migration time varied from 7 to 11.9 min via the increase of DMSO content from 60 to 75 % (see Fig. 3b, d). In contrast, migration time for glutamic acid varied from 13.1 to 13.8 min. This could be a hint to infer that the lower dielectric constant of DMSO is boosting the formation of ion associations between the fast basic amino acids and the anionic CI, producing complexes that migrate at lower velocities than the amino acids dissolved in water or mixed solvents with less content of DMSO.

In the case of electrolyte System B, due to the higher DMSO content, the phenomenon that seemed to be stronger is the shifting of the pI of amino acids, via the strong shift of their $pK_{a(-1)}$. Here, migration time for lysine varied from 10.9 to 11.1 min while for glutamic acid, this variation was from 16.2 to 13.7 when the DMSO content was modified from 80 to 90 % (see Fig. 4b, d). For the electrolyte System B, the effect of DMSO on shifting the pI of the amino acids seemed to be stronger than the shifting of the $pK_{a(-1)}$ of TFA. As a consequence, the difference between the pH of the buffer and the pI of the acidic amino acids is larger, determining a larger proportion of dissociated cationic species, and consequently, higher effective electrophoretic mobilities. Due to the fact that the pI of the basic amino acids is more clearly differentiated from the working pH, the influence of this effect on these analytes is minimal.

In contrast to the mobilities predicted numerically for pure aqueous solutions, when the DMSO content in the solution reaches 80 % for electrolyte System A, and 100 % for electrolyte System B, the mobility window becomes extremely narrow due to the already described ion

association and selective shifting of the $pK_a$ of the amphoteric analytes.

## Application example: NAITP-C$^4$D/CE-MS

In order to implement the NAITP-C$^4$D/CE-MS two-dimensional separation, we use a hybrid capillary-microchip system. This system was successfully tested in a previous work with the implementation of ITP-C$^4$D/CE-MS for the analysis of human angiotensin peptides [11]. In that work, we used a more simple three-port configuration, just using LE as CE-BGE to obtain a comparatively simple setup. In the present study, one goal of the two-dimensional separation was to include independent buffer compositions for both separation steps (BGE independent of LE or TE). For this reason, an extra channel/capillary was required. Consequently, the number of ports to be used for this two-dimensional separation was four: two for the NAITP, and another two for the CE separation as shown in Fig. 1b, and schematically, in Fig. 2.

The results of the NAITP-C$^4$D/CE-MS measurements are shown in Fig. 5a, showing the electric conductivity signal of the NAITP step for the preconcentration of the analytes, and in Fig. 5b, the CE-MS trace with the different EIE's of the 20 amino acids included in the sample and cystine. It is worth mentioning that in this case, due to the fact that the electric conductivity was measured by using the on-chip interface, the resulting electric conductivity scale in this figure is different from the ones shown for the capillary head (Figs. 3 and 4). It is also important to mention that MS recording started after the finalization of the transfer step, as a consequence, the measured time represents analyte migration time from the common channel in the chip interface to the MS, resulting in an overall analysis time of approximately 24 min.

The hybrid system clearly enabled us to perform the NAITP with successful intermediate on-chip C$^4$D detection as shown in Fig. 5. In this case, the on-chip electric conductivity measurement is a more challenging task because of the higher dispersion of the field lines due to the flat-shaped electrodes in comparison with the annular-shaped ones used in the capillary head and the larger distance between the electrolyte solution and the electrodes (130 for 100 µm i.d. capillaries vs. 200-µm lid thickness for the glass chip). Although the signal-to-noise-ratio is clearly not as good as for the capillary detection head, the relative intensities for LE and TE are clearly differentiated, enabling the detection of the arrival of the sample stack at the intersection for triggering the switching of the electric potential on Port 3 to start the transfer step (see "Materials and methods" section).

The sample transfer was efficiently performed in the hybrid system, as far as all the analytes reached the MS at the end of the CE separation capillary due to the advantage of having an extreme narrow mobility window for the NAITP step (for the relatively low concentration used; at higher concentration, ITP separation of analytes becomes visible). The clear drawback of this implementation is that CE-MS separation was not fully reached for the 20 sample components as is clearly shown in Fig. 5. This incomplete separation can be attributed to the incomplete replacement of DMSO in the second dimension. It is possible that the dilution process was not fast enough due to the high viscosity ($\eta \approx 2$ mPa · s) of both solutions (sample with 20:80 water/DMSO and BGE with 80:20 water/2-propanol). The presence of a high content of DMSO in the sample plug decreases the efficiency of the recovery process of the aqueous mobilities. Nevertheless, the migration order of the analytes is coherent with the numerically predicted one, which demonstrates that the replacement of DMSO is occurring, but not completely.

Another important aspect of sample transfer refers to switching times for transferring sample from the first dimension to the second. If the switching from the NAITP

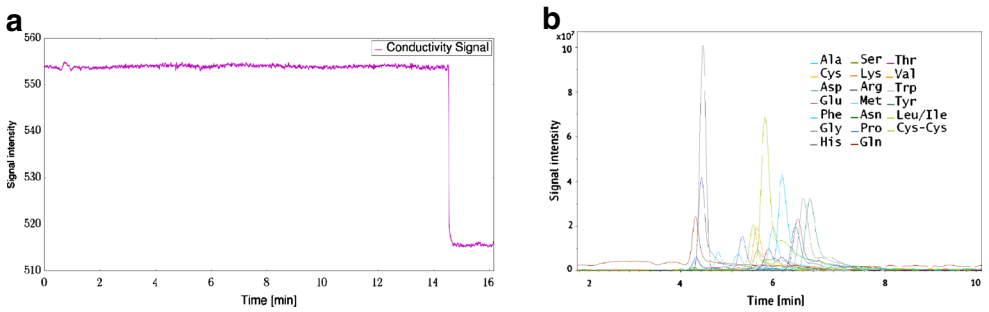


**Fig. 5** NAITP-C$^4$D/CE-MS results, by means of C$^4$D signal trace and EIE's for the 20 amino acids present in the sample plus cystine. Experimental conditions: NAITP using electrolyte System A with 80 % DMSO (see Table 1) and CE using 20 mM oxalic acid in a solution of 80:20 water/2-propanol. Hydrodynamic and electrical parameters were: 7 s at 100 mbar for injection, +30 kV for NAITP, and +15 kV for CE separation. (**a**) cITP with C$^4$D signal. (**b**) CE-MS with EIE

to the transfer process occurs too early, a large amounf of LE will be transferred to the second dimension in front of the sample. In a similar way, if the switching from the transfer process to the CE step is performed after the optimal time point, a fraction of TE will follow the sample in the CE separation. Due to this, a transient ITP system continues migrating in the CE buffer slowing down the unstacking process. We want to stress that a partial transfer of LE and TE within the sample is also advantageous to some extent, due to the fact that some stacking effects provide sharper CE peaks, though precise timing has to be accomplished. The trade-off on how much LE and TE are transferred with the sample to the second dimension in two-dimensional electrophoretic separations involving ITP as first dimension, has ever been a critical parameter to be optimized [8, 25].

In Fig. 5, it is worth noting that different groups of analytes are separated in concordance with the predicted mobilities for aqueous solutions: the first group contains the basic amino acids lysine, histidine and arginine; the second includes the low molecular weight alanine, glycine and valine; then a large group of several amino acids not well separated and finally, the acidic (glutamic acid and aspartic acid) and the large aromatic ones (phenylalanine, tyrosine and tryptophan).

Besides the optimization of the transfer process to enhance this separation, different strategies can be adopted; for example increase the electric field by increasing the separation voltage (in our case this would imply the development of a new voltage source), increase the length of the separation capillary enabling the increase of the diffusion of the DMSO into the CE buffer, or include some complexation agents, in the CE buffer that already demonstrated to be useful for amino acid analysis [1, 26].

## Conclusions

In this work, we developed a relatively simple view on isotachophoresis using conductivities to describe the isotachophoretic conditions. These include the conductivity of the $H^+$, which is understood as an overlay of Stokesian migration and EZE flipping mechanism. In order to fulfill the ITP conditions, we addressed every conductivity term by using the dipolar aprotic solvent DMSO. With DMSO, cationic ITP becomes feasible as the electrophoretic analyte mobility and thus its conductivity is increased due to the stabilization of the cations in this solvent, the conductivity due to the counterion is decreased because of the destabilization of anions in DMSO. Most importantly, hydrogen bonds are strongly reduced prohibiting the EZE flipping mechanism. Together with the very high autoprotolysis constant of DMSO, a very low conductivity due to the protons evolves. Only then can proper ITP conditions evolve with oxalate and TFA as counterions and weak bases (or ampholytes of low pI) as analytes. Using mass spectrometric detection in conjunction with $C^4D$, the composition of each zone was determined and it is clear that $H^+$ was real TE in the system.

In this work, a comprehensive NAITP for the 20 proteinogenic amino acids was presented for the first time, which is also applicable to weak bases bases such as amino- and diamino-benzoic acid (data not shown). The addition of LE and CI to the sheath liquid enabled us to perform direct ESI-MS detection of cationic ITP avoiding the use of external hydrodynamic pressure for step mobilization. As an application example of the NAITP method developed in this work, it was integrated into a two-dimensional electrophoretic separation of NAITP-on-chip-$C^4D$/CE-MS in a hybrid capillary-microfluidic setup used previously in a simpler configuration, now enabling a CE-BGE independent of the ITP electrolytes. Clearly, the sample transfer was successful due to the very narrow ITP stack. The CE-MS analysis as well as the transfer procedure still have to be further optimized, but we believe that the method developed will be very important for future preconcentration strategies for electromigrative and even other separation techniques. This can either be achieved in a transient format, where the sample may simply be injected in DMSO, or as was successfully demonstrated in the present study, in a column-coupled mode.

*Electronic supplementary material* this paper is completed with information and discussions included in a Supplementary Material. A complete discussion about the validity of ITP Conditions (1) and (2), as well as a novel description of ITP stacking process based on conductivities (instead of the classical one based on mobilities) can be found. Also, a description of DMSO physicochemical properties and how these properties enable the fulfillment of ITP conditions at extremely low pH values is presented. We strongly recommend readers interested in fundamentals on bioanalytical physicochemistry to access this Supplementary Material.

**Acknowledgments** This work was funded by the Excellence Initiative, a jointly funded program of the German federal and state governments, organized by the German Research Foundation (DFG) and by the Initiative and Networking Fund of the Helmholtz Association within the framework of the Helmholtz Young Investigators Group Program. We also want to thank Tjorben Posch, Daniel Sydes and Uwe Breuer (ZEA-3, Forschungszentrum Jülich), Maria Matveeva (IEK-4, Forschungszentrum Jülich), Daniel Lutz, and Peter Zipfl (CalvaSens GmbH, Aalen), and Matthias Bauerfeind for their valuable collaboration.

## References


1. Chiu T-C (2013) Anal Bioanal Chem 405:7919–7930
2. Loo JA, Udseth HR, Smith RD (1989) Anal Biochem 179(2):404–412
3. Gebauer P, Malá Z, Boček P (2009) Electrophoresis 30(1):29–35
4. Kler PA, Sydes D, Huhn C (2014) Anal Bioanal Chem. doi:10.1007/s00216–014–8099–7
5. Holloway CJ, Pingoud V (1981) Electrophoresis 2(3):127–134
6. Baidoo EE, Benke PI, Neusüss C, Pelzing M, Kruppa G, Leary JA, Keasling JD (2008) Anal Chem 80(9):3112–3122
7. Davis NI, Mamunooru M, Vyas CA, Shackman JG (2009) Anal Chem 81(13):5452–5459
8. Boček P, Deml M, Gebauer P, Dolník V (1988) Analytical isotachophoresis. Wiley-VCH, Weinheim
9. Soga T, Kakazu Y, Robert M, Tomita M, Nishioka T (2004) Electrophoresis 25(13):1964–1972
10. Kubáň P, Boček P (2012) J Chromatogr A 1234:2–8
11. Kler PA, Posch TN, Pattky M, Tiggelaar RM, Huhn C (2013) J Chromatogr A 1297(5):204–212
12. Malá Z, Gebauer P, Boček P (2013) Electrophoresis 34(1):19–28
13. Kler PA, Berli CL, Guarnieri FA (2011) Microfluid Nanofluid 10(1):187–198
14. Kler PA, Dalcin LD, Paz RR, Tezduyar TE (2013) Comput Mech 51(2):171–185
15. Tiggelaar R, Benito-Lopez F, Hermes D, Rathgen H, Egberink R, Mugele F, Reinhoudt D, van den Berg A, Verboom W, Gardeniers H (2007) Chem Eng J 131(1-3):163–170
16. Tanaka Y, Matsuda Y, Fujiwara H, Kubota H, Makita T (1987) Int J Thermophys 8(2):147–163
17. Laque WE, Ronneberg CE (1970) Ohio J Sci 70(2):97–106
18. Otaka A, Koide T, Shide A, Fujii N (1991) Tetrahedron Lett 32(9):1223–1226
19. Koide T, Otaka A, Fujii N (1993) Chem Pharm Bull 41(6):1030–1034
20. Brito-Neto JGA, Fracassi daSilva JA, Blanes L, doLago CL (2005) Electroanal 17(13):1198–1206
21. Markovitch O, Chen H, Izvekov S, Paesani F, Voth GA, Agmon N (2008) J Phys Chem B 112(31):9456–9466
22. Saito RM, Brito-Neto JGA, Lopes FS, Blanes L, daCosta ET, Vidal DTR, Hotta GM, doLago CL (2010) Anal Methods 2(2):164–170
23. Gileadi E, Kirowa-Eisner E (2006) Electrochim Acta 51(27): 6003–6011
24. Porras SP, Riekkola M-L, Kenndler E (2003) Electrophoresis 24(10):1485–1498
25. Everaerts FM, Beckers JL, Verheggen TP (1976) Isotachophoresis: theory instrumentation and applications. Elsevier, Amsterdam
26. Britz-McKibbin P, Terabe S (2003) J Chromatogr A 1000(1–2): 917–934